Electron Ejection from Single Crystals Due to 1- to 10-keV Noble-Gas Ion Bombardment

C. E. CARLSTON, G. D. MAGNUSON, P. MAHADEVAN
Space Science Laboratory, General Dynamics/Convair, San Diego, California

AND

D. E. HARRISON, JR.
Department of Physics, U. S. Naval Postgraduate School, Monterey, California

(Received 25 January 1965; revised manuscript received 7 April 1965)

The secondary-electron ejection coefficient γ has been measured for the (110), (100), and (111) planes of Cu, Al, Ag, Ni, and Mo bombarded by the singly charged noble-gas ions Ne^+, Ar^+, Kr^+, and Xe^+ in the energy range from 1 to 10 keV. Surfaces were kept clean to within a fraction of a monolayer contamination by the sputtering action of the incident ion beams. The ratios $\gamma_{hkl}/\gamma_{h'k'l'}$ are quite constant, which would tend to indicate a theoretical model based on simple geometrical considerations of the opacity of the single-crystal planes. However, the fact that the ratios are relatively insensitive to the ion-bombardment energy indicates that a model based upon the transparency of the target is not sufficient to explain the phenomenon. The dependence of γ on the bombarding-ion mass is also explored.

INTRODUCTION

ALTHOUGH there are considerable data available on the secondary-electron ejection coefficients γ for many polycrystalline target materials by many bombarding ions,[1] little data have been obtained[2–5] using single crystals of various metals. The preliminary results in Ref. 5 (hereafter referred to as Paper II) suggested that one of the important parameters of the phenomenon of secondary-electron emission is the opacity of the crystal as seen by the incident ion beam. The results of Paper II seemed also to indicate that since a cross section of interaction between a neutralized projectile atom and a target atom could be assumed, ionization of the projectile atoms was taking place, leading to the ejection of electrons. The theoretical description presented in the following paper[6] shows that the opacity concept does not describe the process, but supports the conjecture that the projectile ions supply the ejected electrons. It was the purpose of the present paper, however, to obtain data that would reveal other important facets of secondary-electron emission such as the dependence of γ on the bombarding-ion mass, as well as to corroborate or refute the results of Paper II for Ar^+ ions bombarding the low-index planes of Cu.

APPARATUS AND PROCEDURE

The apparatus used in these experiments has been described in detail in a previous paper[7] (hereafter referred to as Paper I). The apparatus consists of (1) an ion source the characteristics and operation of which have previously been reported,[8] (2) a stainless-steel target chamber 14 in. in diameter and 18 in. long capable of achieving vacua of 1 to 4×10^{-8} Torr, in which background pressure the experiments were performed, and (3) a target collector system which was used to hold and orient the targets and to measure the secondary-electron emission coefficient γ. See Fig. 1 of Paper I. The ion-

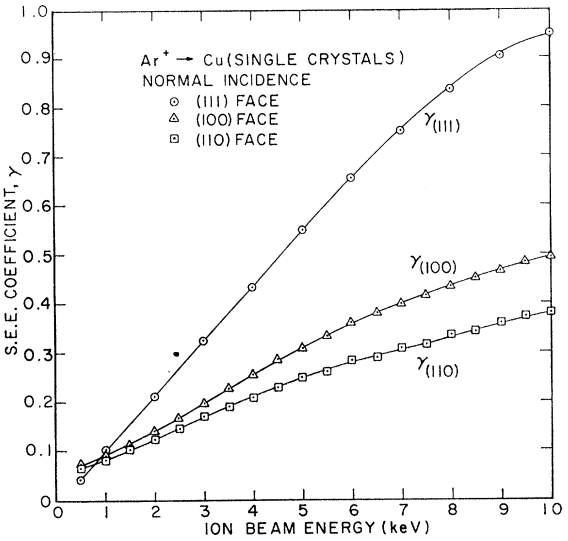

FIG. 1. Secondary-electron emission coefficient for Ar^+ ions incident on the three low-index planes of Cu, as a function of ion energy.

[1] H. D. Hagstrum, Phys. Rev. **89**, 244 (1953); **96**, 325 (1954); **104**, 672 (1956); **104**, 317 (1956); **119**, 940 (1960); **96**, 336 (1954); **104**, 1516 (1956); J. Appl. Phys. **32**, 1015 (1961); W. Ploch, Z. Physik **130**, 174 (1951); N. N. Petrov, Fiz. Tverd. Tela **2**, 1300, 940, 949 (1960) [English transls.: Soviet Phys.—Solid State **2**, 1182, 857, 865 (1960)]; É. S. Parilis and L. M. Kishinevskii, Fiz. Tverd. Tela **3**, 1219 (1960) [English transl.: Soviet Phys.—Solid State **3**, 885 (1960)]; O. V. Roos, Z. Physik **147**, 210 (1957); N. N. Petrov and A. A. Doroghkin, Fiz. Tverd. Tela **3**, 53 (1961) [English transl.: Soviet Phys.—Solid State **3**, 38 (1961)].

[2] Y. Takeishi and H. D. Hagstrum (private communication).

[3] B. Fagot and C. Fert, Compt. Rend. **258**, 1180 (1964).

[4] B. Fagot, N. Colombie, and C. Fert, Compt. Rend. **258**, 4670 (1964).

[5] G. D. Magnuson and C. E. Carlston, Phys. Rev. **129**, 2409 (1963).

[6] D. E. Harrison, Jr., C. E. Carlston, and G. D. Magnuson, following paper, Phys. Rev. **139**, A737 (1965).

[7] G. D. Magnuson and C. E. Carlston, Phys. Rev. **129**, 2403 (1963).

[8] C. E. Carlston and G. D. Magnuson, Rev. Sci. Instr. **33**, 905 (1962).

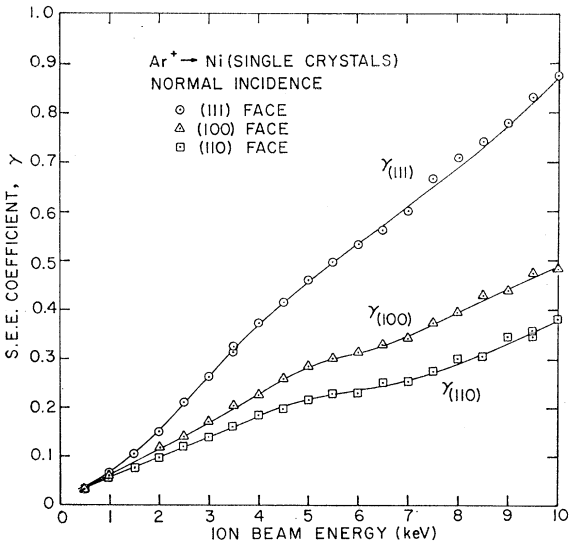

FIG. 2. Secondary-electron emission coefficient for Ar^+ ions incident on the three low-index planes of Ni, as a function of ion energy.

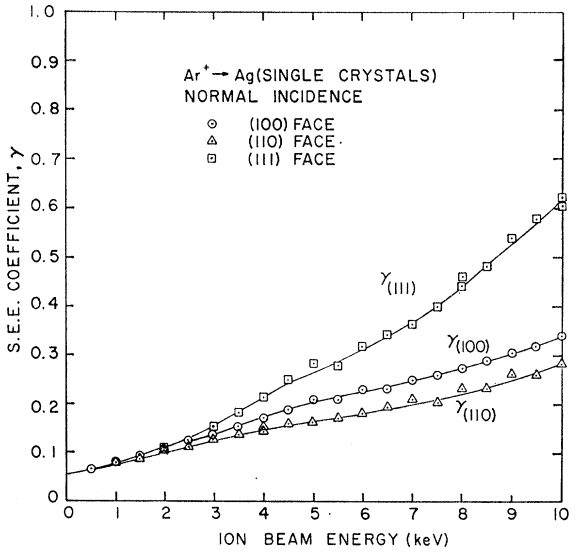

FIG. 4. Secondary-electron emission coefficient for Ar^+ ions incident on the three low-index planes of Ag, as a function of ion energy.

beam purity was >97%. For this reason magnetic analysis of the ion beam was not used. The total energy spread of the ion beam was ≤ 3 eV. Energetic neutrals or metastables were determined to comprise less than 0.01% of the total beam current. The secondary-electron collector was a sphere 3 in. in diameter with the target located at its center.

Prior to bombardment of the targets, the ion source was prepared for operation by a procedure somewhat akin to "baking out." For this reason the procedure is named source bakeout and involves a cleaning of the ion source by heating to reduce the impurity content of the ion beam. In addition, a discharge is run for one hour before measurements of γ are made. This procedure is fully explained in Paper I.

When changing from one gas to another, the complete procedure of source preparation is somewhat more extensive. Prior to bakeout, the source pressure is increased to approximately 20 μ of Hg for several minutes to purge the source and gas feed system. The bakeout procedure is completed, followed by 20 h of ion extraction and source operation. After 4 h of operation, the beam purity required is achieved. The target is

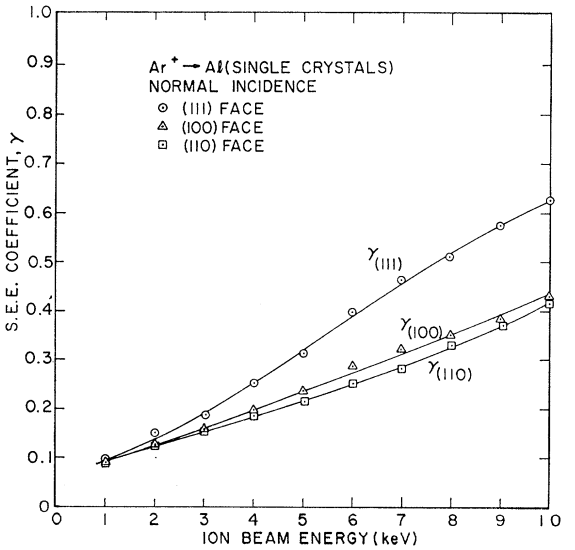

FIG. 3. Secondary-electron emission coefficient for Ar^+ ions incident on the three low-index planes of Al, as a function of ion energy.

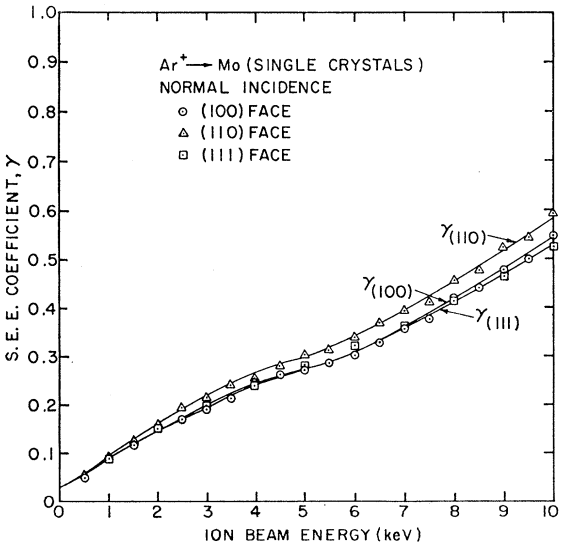

FIG. 5. Secondary-electron emission coefficient for Ar^+ ions incident on the three low-index planes of Mo, as a function of ion energy.

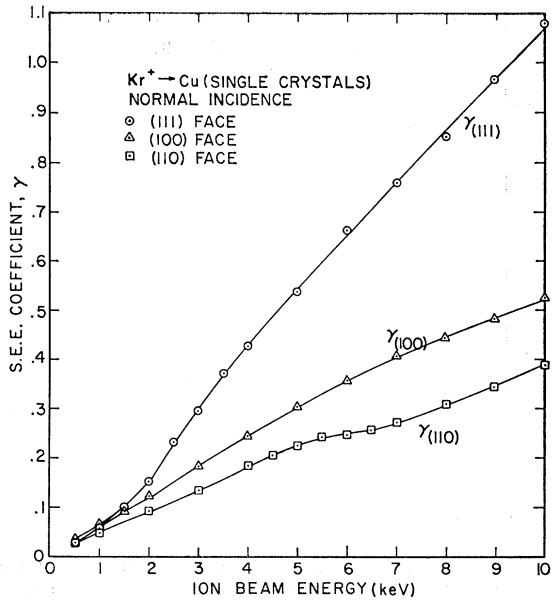

FIG. 6. Secondary-electron emission coefficient for Kr^+ ions incident on the three low-index planes of Cu, as a function of ion energy.

bombarded at several keV until clean, as evidenced by a constant value of γ with bombardment time and bombardment current density. The techniques used to determine surface cleanliness are described in detail in Paper I and involve techniques such as monolayer formation times and curves of γ versus incident-ion-beam current density.

Target surfaces are kept clean by ion bombardment, resulting in an atom-removal rate due to sputtering which exceeds the contaminant arrival and sticking rate from ambient. This technique has been explained fully in Paper I.

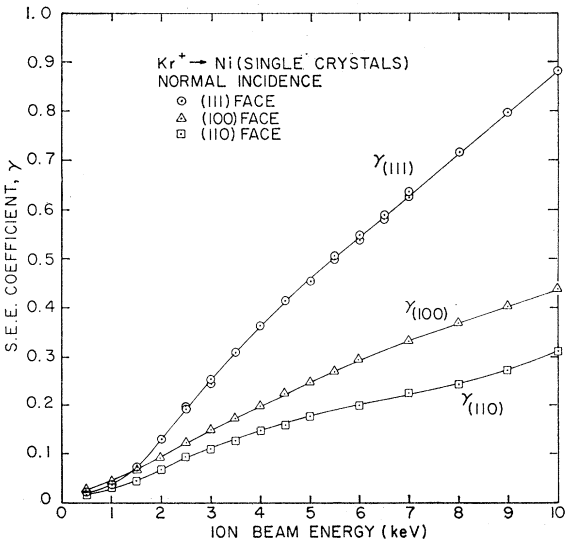

FIG. 7. Secondary-electron emission coefficient for Kr^+ ions incident on the three low-index planes of Ni, as a function of ion energy.

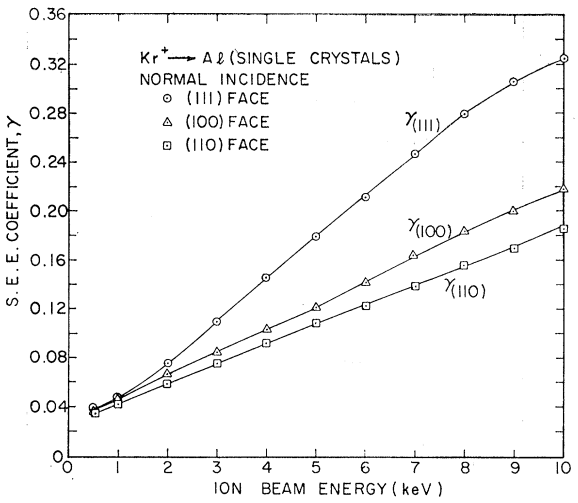

FIG. 8. Secondary-electron emission coefficient for Kr^+ ions incident on the three low-index planes of Al, as a function of ion energy.

The basic procedure for measuring γ has been reported in Papers I and II. With the exception of Mo and Cu, all single crystals used in this work were purchased from two outside sources. The Cu crystals were grown, cut, and oriented to within 1° in this laboratory. The Mo crystals were cut and oriented in this laboratory from crystal rod purchased from an outside source. They were within 1° of desired orientation. The purchased crystal orientations were all within 2° of the orientation required and were bombarded at an angle within $\frac{1}{4}$° of normal incidence.

The procedure involving the crystals of Ag, Al, and Ni

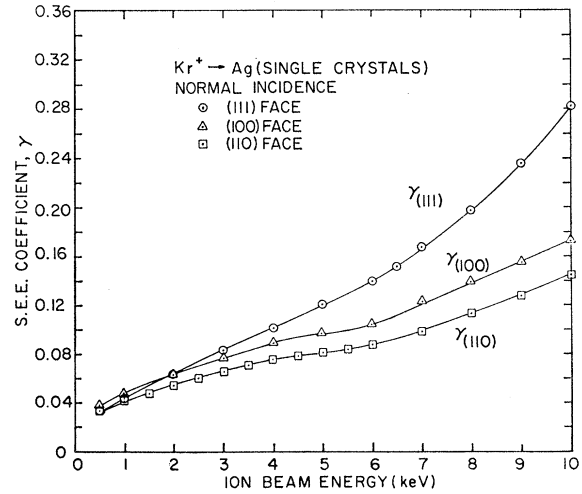

FIG. 9. Secondary-electron emission coefficient for Kr^+ ions incident on the three low-index planes of Ag, as a function of ion energy.

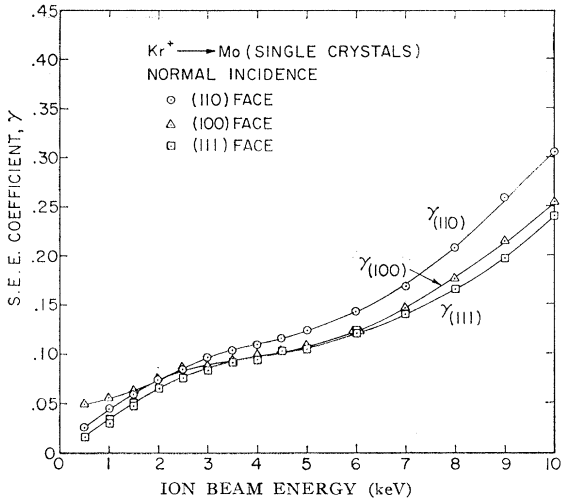

FIG. 10. Secondary-electron emission coefficient for Kr^+ ions incident on the three low-index planes of Mo, as a function of ion energy.

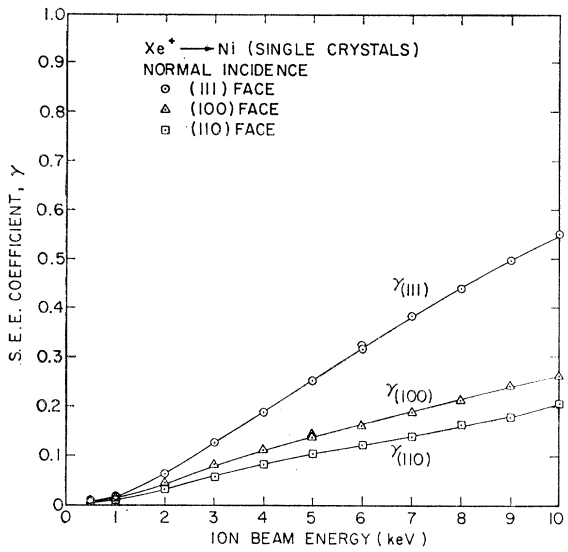

FIG. 12. Secondary-electron emission coefficient for Xe^+ ions incident on the three low-index planes of Ni, as a function of ion energy.

was the following: (1) The crystals were etched in an appropriate etchant for the material to remove the cold-worked surface, (2) deposit spot patterns were made to determine the conditions of the surface (obtaining a spot pattern due to a single crystal indicates that the surface of the material as well as the bulk is single crystal and not cold worked), (3) Laue back-reflection photographs were taken of the crystal using an X-RD-5 x-ray machine to determine the orientation of the crystal, (4) the crystals were washed in distilled water and alcohol before installing in the vacuum system.

Recently the authors have analyzed the positive-ion reflection component that is observed when the collector is biased negatively.[9] The authors have, as a result of that work, come to the conclusion that the positive-ion reflection coefficient is more properly a metastable-atom-formation coefficient. Therefore γ should be calculated from the relation $\gamma=I_c/(I_t-I_c)$ rather than from the relation $\gamma=(I_c+I_R)/(I_t-I_c)$ as was done in Papers I and II where I_c is the collector current, I_t is the target current, and I_R is the "reflected ion current." Since metastable atoms would eject low-energy electrons from the collector that would be collected by the target in the reverse-bias configuration, they would appear to be positive ions reflected from the target. These low-

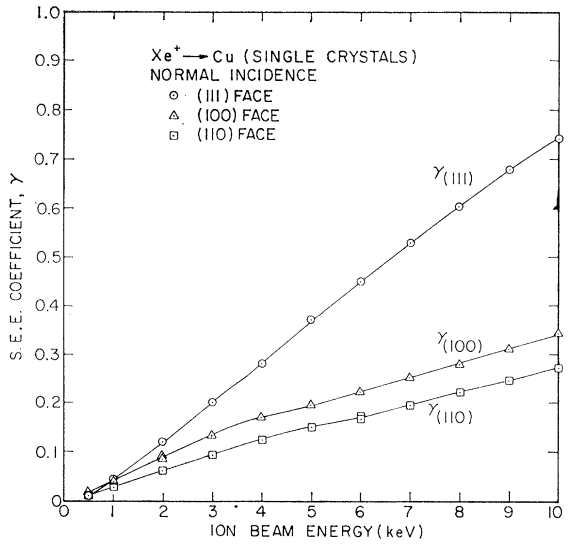

FIG. 11. Secondary-electron emission coefficient for Xe^+ ions incident on the three low-index planes of Cu, as a function of ion energy.

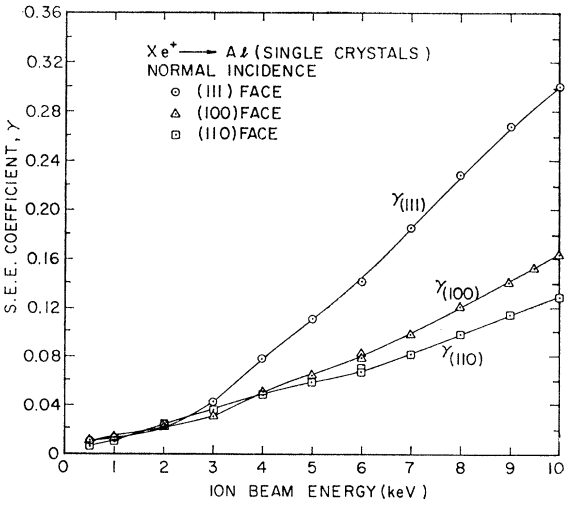

FIG. 13. Secondary-electron emission coefficient for Xe^+ ions incident on the three low-index planes of Al, as a function of ion energy.

[9] C. E. Carlston and G. D. Magnuson, Bull. Am. Phys. Soc. 8, 77 (1963).

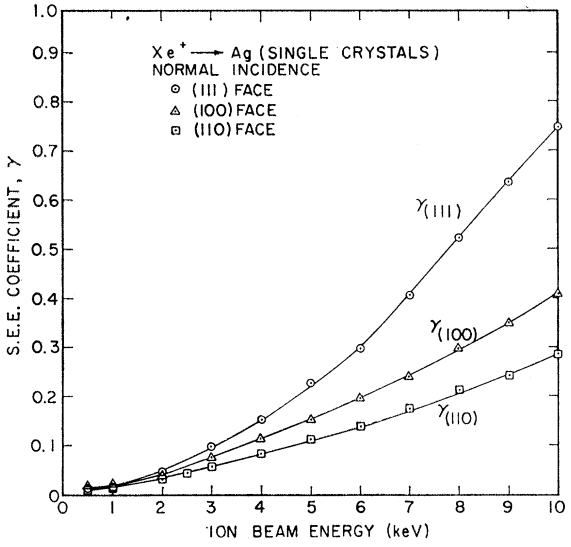

FIG. 14. Secondary-electron emission coefficient for Xe^+ ions incident on the three low-index planes of Ag, as a function of ion energy.

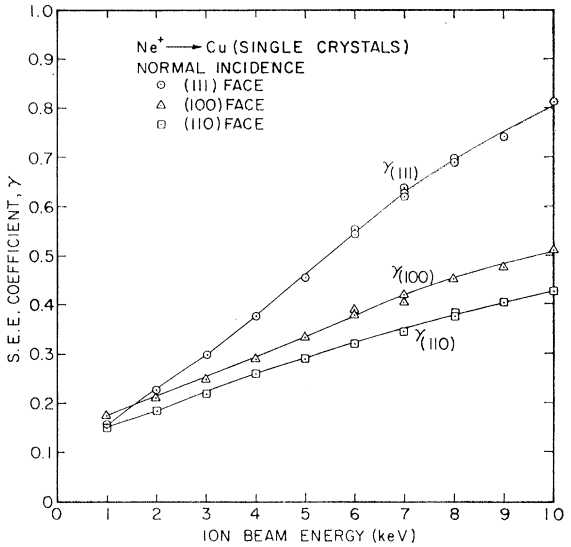

FIG. 16. Secondary-electron emission coefficient for Ne^+ ions incident on the three low-index planes of Cu, as a function of ion energy.

energy electrons would be retarded with a few volts positive on the collector and the current would not need to be added to the collector current in the calculation of γ as is the case with reflected, high-energy ions. The difference in γ, due to the small magnitude of the reflection coefficient ($<1\%$) is at most 5% at low energies and even less at high energies. The values of γ for Ar^+ on Cu monocrystals have been adjusted as presented here to account for this difference.

The maximum expected uncertainty in the values of γ reported here is $\pm 7\%$ and the reproducibility of results under widely varying conditions was found to be $\pm 3\%$.

RESULTS AND DISCUSSION

Dependence on Ion Energy and Crystal Orientation

The values of the secondary-electron emission coefficient γ are shown in Figs. 1 through 19 in the energy range 500 eV to 10 keV for bombardment of the (110), (100), and (111) faces of Al, Ag, Cu, Mo, and Ni by Ne^+, Ar^+, Kr^+, and Xe^+. The sputtering yield of the combination $Ne^+ \rightarrow Al(h,k,l)$ is so small that the clean-surface values of γ could not be measured in this energy range and at the background pressure and current densities attainable in the present apparatus. For completeness

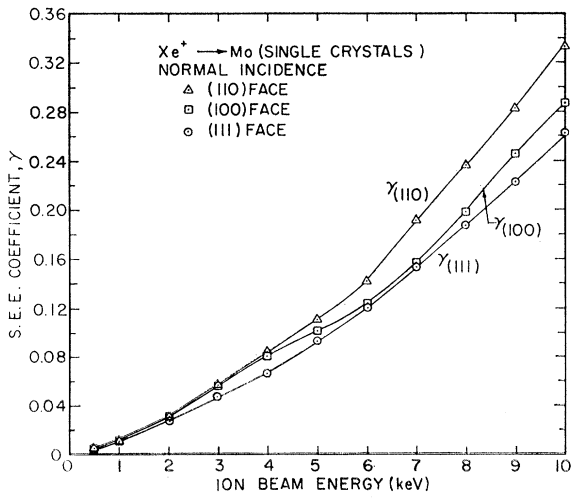

FIG. 15. Secondary-electron emission coefficient for Xe^+ ions incident on the three low-index planes of Mo, as a function of ion energy.

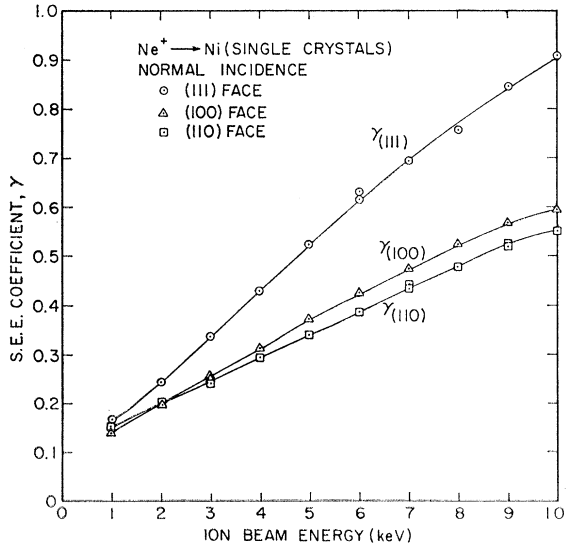

FIG. 17. Secondary-electron emission coefficient for Ne^+ ions incident on the three low-index planes of Ni, as a function of ion energy.

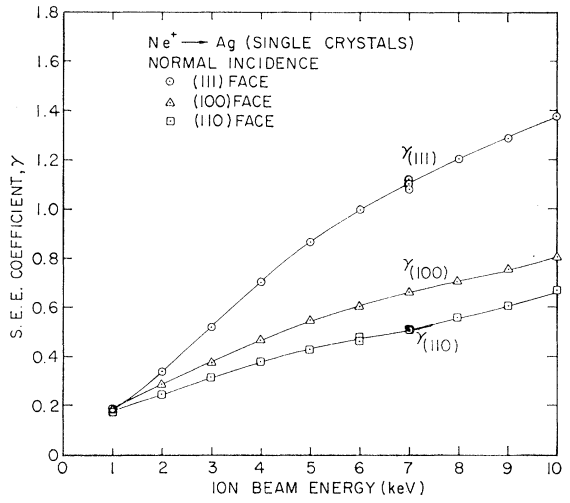

FIG. 18. Secondary-electron emission coefficient for Ne^+ ions incident on the three low-index planes of Ag, as a function of ion energy.

the revised curves for Ar^+ bombarding the low-index planes of Cu have been included. It should be noted that with few exceptions the secondary-electron-emission coefficient of the (111) face of the fcc crystals studied is not significantly greater than the yield of the (100) face at energies below roughly 1 keV. This would imply that at low energies a model based on the transparency of the crystal planes, as was explored in Paper II, is not sufficient to account for the ordering of the γ values from different crystal planes.

The effect of crystalline orientation of the target was observed for every metal studied. The ratios of the yields of the three low-index planes of each metal studied were calculated and plotted versus energy as was done

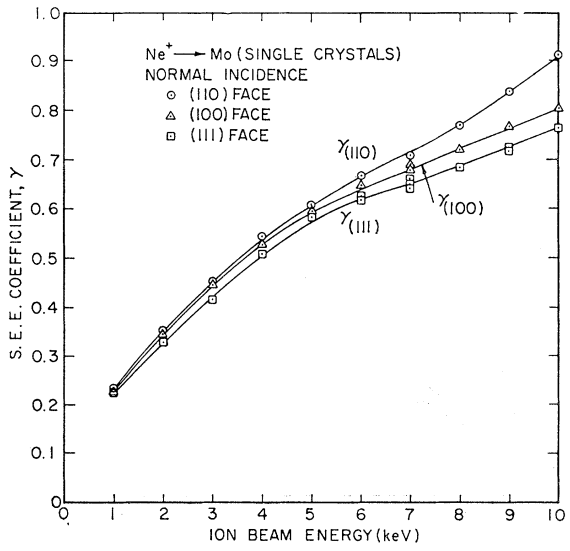

FIG. 19. Secondary-electron emission coefficient for Ne^+ ions incident on the three low-index planes of Mo, as a function of ion energy.

TABLE I. The ratios of the γ values of different crystal planes for the fcc metals investigated. The percent deviation is the percentage difference from the mean. The average values of all the ion-metal combinations are given in the last row of the table.

Ion-metal combination	Ratios of $\gamma(i,j,k)/\gamma(l,m,n)$ $\gamma(111)/\gamma(110)$ Value	% dev.	$\gamma(111)/\gamma(100)$ Value	% dev.	$\gamma(100)/\gamma(110)$ Value	% dev.
$Ar^+ \rightarrow Ni$	2.48	+2.48	1.82	−1.1	1.38	+6.2
$Ar^+ \rightarrow Ag$	2.44	+0.83	1.71	−7.1	1.30	0
$Ar^+ \rightarrow Cu$	2.68	+10.8	1.89	+2.7	1.41	+8.5
$Ar^+ \rightarrow Al$	1.80	−25.6	1.60	−13.0	1.12	−21.5
$Kr^+ \rightarrow Ni$	2.90	+19.8	1.95	+6.0	1.45	+11.5
$Kr^+ \rightarrow Ag$	2.12	−12.4	1.71	−7.1	1.20	−7.7
$Kr^+ \rightarrow Cu$	2.77	+14.5	2.02	+9.8	1.38	+6.2
$Kr^+ \rightarrow Al$	1.96	−18.6	1.60	−13.0	1.22	−6.2
$Xe^+ \rightarrow Al$	2.36	−2.5	1.86	+13.0	1.26	−3.1
$Xe^+ \rightarrow Cu$	2.67	+10.3	2.18	+18.5	1.23	−5.4
$Xe^+ \rightarrow Ag$	2.63	+8.7	1.82	−1.1	1.44	+10.8
$Xe^+ \rightarrow Ni$	2.68	+10.8	2.08	+13.0	1.29	−0.8
$Ne^+ \rightarrow Ag$	2.55	+5.4	1.85	+0.5	1.40	+7.7
$Ne^+ \rightarrow Ni$	1.80	−25.6	1.54	−16.3	1.19	−8.5
$Ne^+ \rightarrow Cu$	2.40	−0.83	1.96	+6.5	1.21	−6.9
Average	2.42	14.2	1.84	9.6	1.30	6.96

in Paper II. Tables I and II show the values of the ratios above 6 keV for the various combinations studied. The mean deviations of all of these ratios is well within experimental uncertainty, but individual deviations are often quite large, so it appears that additional factors enter into the mechanism of secondary-electron emission. Since the variation with incident-ion energy of the potential-ejection contribution to γ for the cases studied here is not known, it is difficult to predict what effect potential ejection has on the results at the higher energies. It is tacitly assumed that, at the higher energies, $\gamma_{P.E.}$ becomes negligible in comparison to $\gamma_{K.E.}$ and need not be considered in these calculations. However, it is apparent from the work of Takeishi and Hagstrum[2] in the potential-ejection range that the variation of $\gamma_{P.E.}$ with energy is not simple. In order to determine the variation of $\gamma_{P.E.}$ with energy, the kinetic-ejection coefficient by ground-state neutral atoms $\gamma_{K.E.}$ must be measured and subtracted from the total secondary-electron emission coefficient due to ions. An experiment of such a nature would determine whether disagreement between the opacity-model predictions and measured values is due partly to the effect of potential ejection. The values of γ for argon ions and neutrals bombarding Mo have been measured by

TABLE II The ratios of the γ values of different crystal planes for Mo. The percent deviation is the percentage difference from the mean. The average values are given in the last row of the table.

Ion-metal combination	Ratios of $\gamma(i,j,k)/\gamma(l,m,n)$ $\gamma(110)/\gamma(111)$ Value	% dev.	$\gamma(110)/\gamma(100)$ Value	% dev.	$\gamma(100)/\gamma(111)$ Value	% dev.
$Ne^+ \rightarrow Mo$	1 23	+0 82	1.16	+0.87	1.06	0
$Ar^+ \rightarrow Mo$	1.10	−9.83	1.10	−4.33	1.02	−3.77
$Kr^+ \rightarrow Mo$	1.27	+4.10	1.19	+3.47	1.05	−0.94
$Xe^+ \rightarrow Mo$	1.28	+4.50	1.17	+1.74	1.10	+5.60
Average	1.22	5.89	1.15	2.94	1.06	2.70

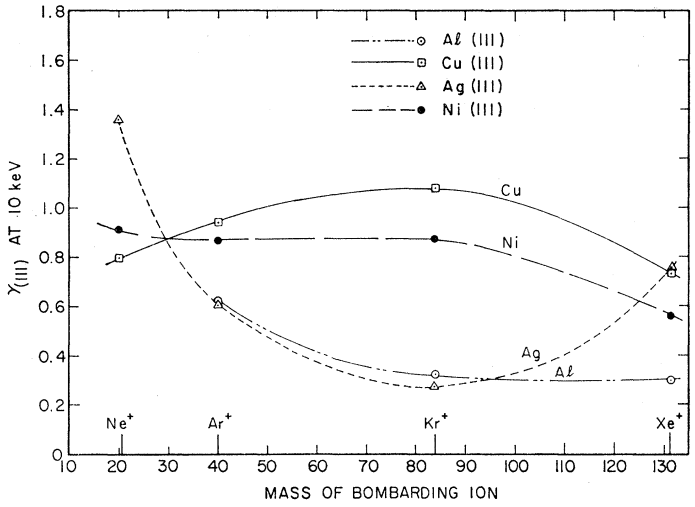

FIG. 20. The secondary-electron emission coefficient of the fcc single crystals studied in this research plotted as a function of the mass of the bombarding ion. The γ values are those for 10-keV ions incident on the (111) plane.

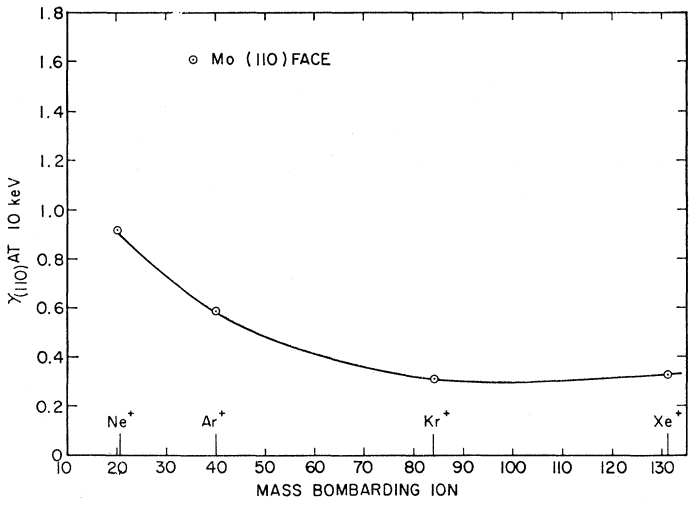

FIG. 21. The secondary-electron emission coefficient for the (110) face of Mo plotted as a function of the mass of the bombarding ion and an ion energy of 10 keV.

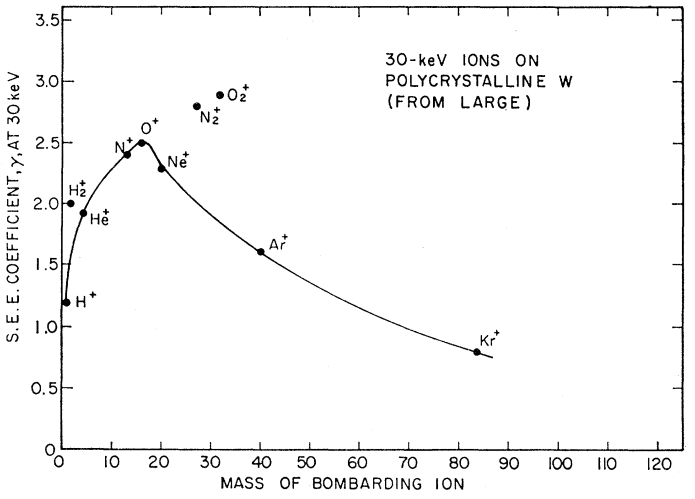

FIG. 22. The data of Large (Ref. 11) showing the secondary-electron emission coefficient at 30-keV incident ion energy, plotted as a function of the mass of the bombarding ion.

Medved, Mahadevan, and Layton[10] in such an experiment, however, the upper limit of their energy range was 2500 eV. Their results indicate that for the combination Ar → Mo, the potential-ejection coefficient $\gamma_{P.E.}$ is flat from 100 to 700 eV and then appears to be monotonically increasing with energy. The theoretical paper

[10] D. B. Medved, P. Mahadevan, and J. K. Layton, Phys. Rev. **129**, 2086 (1963).

provides evidence that the ion and neutral-atom experiments should be quite similar. In both cases the electron-production mechanism involves a neutral atom and a lattice "atom." In the neutral-bombardment experiment the atom is known to be in the ground state while in the ion-bombardment experiment there is a possibility that the neutralization is into an excited state. The simultaneous operation of the potential-ejection and kinetic-ejection mechanisms need further study. The low-energy portions of these experiments is particularly difficult to explain, and further theoretical analysis is clearly indicated.

In many, but not all, of the curves reported here, there appears to be a small hump at an energy of from 4 to 7 keV. This hump may be present in the curves for one or two faces of a crystal and not in the others. There seems to be no clearly defined relationship between the variables involved in the experiment and the appearance of these humps. The existence of a hump in a curve may possibly be explained by a rather abrupt decrease of the potential-ejection coefficient at the energy of appearance of the hump, causing the total electron-ejection coefficient to exhibit a change in slope and an inflection point giving the appearance of a hump. It is also possible that the hump may be real and be the result of resonant ionization of the target atom. In any case, it is not clear why there should be a difference between the behavior of the curves for different crystal planes of the same metal crystal. The behavior of $\gamma_{P.E.}$ throughout this energy range would be of interest in explaining the appearance of humps in these curves.

Dependence of γ on Mass of Bombarding Ion

Figure 20 shows a plot of γ versus the mass of the bombarding ion M_i. Similar plots are obtained if γ is plotted versus the ionization potentials of the bombarding ions. The yield values are those of the (111) plane of various fcc target materials at an incident-ion energy of 10 keV. Figure 21 is the same plot for the (110) plane of a Mo single crystal. Since the effect of crystalline orientation is only to change the yield values by a constant multiplicative factor, similar plots for the (110) and (100) planes would exhibit the same characteristics but with the scale for γ decreased by factors of 2.45 and 1.73, respectively.

There is an intersection of the curves at a mass of roughly 29 which would indicate that a bombarding ion of mass 29 would have the same yield from all the metals investigated. These same curves have been plotted using the values of γ at a velocity of 12.1×10^4 m/sec (the velocity of a 10-keV Xe^+ ion). The intersection at mass 29 was still present. The result thus is that an ion of mass 29 would have the same yield for all (111) fcc planes investigated both at a constant energy of 10 keV and at a constant velocity of 12.1×10^4 m/sec. Without further theoretical investigation it is difficult to explain this result. Similar curves for polycrystalline Cu, Ta, and Mo were made. The shapes of the Ta and Mo curves agreed with the shapes of the curves for the (110) face of Mo. The shape of the curve for polycrystalline Cu agreed with the curve for the (111) face of Cu. The scale of γ was of course different. Figure 22 shows a similar plot of the work of Large.[11] The points are his values for He^+, Ne^+, Ar^+, Kr^+, H_2^+, H^+, N_2^+, and O_2^+ bombarding polycrystalline W at an energy of 30 keV. It is possible to draw a smooth curve through the points which is similar to Fig. 21 (above mass 20) if one discards the points for H_2^+, N_2^+, and O_2^+. This, coupled with the fact that the H_2^+, N_2^+, and O_2^+ points all lie above the curve, suggest that the molecular species may have possessed appreciable energies in the form of metastable molecular excitation which would then contribute to secondary-electron emission in much the same way that metastable atoms do. It is possible to plot such curves for the work of Petrov and Dorohzkin[12] and Tel'kovskii[13] which are quite similar. Neglecting the molecular species, the work of Large, Petrov and Dorozhkin, Tel'kovskii, and this work agree with regard to the shapes of the curves for masses including and above Ne^+ for bcc metals. Tel'kovskii's values are approximately 2 times as high as those in this work for polycrystalline Mo. Recent work by Daly and Powell[14] using 40-keV noble-gas ions on polycrystalline Al seems to be in disagreement with other work in that the peak appears at mass 40 rather than mass 20. Their curves also show a minimum at mass 84. In order to fully describe the dependence of γ on the mass of the bombarding ion, it is obvious from the work of Large that the present measurements must be extended to lower mass ions. This work must include ions of N^+, O^+, He^+, and H^+ on the various targets investigated as well as Ne^+ on Al. The technique used in this work requires that the bombarding ion beam clean the target surface as well as eject secondary electrons. In order for the ion beam to clean the target by sputtering, the background pressure, sticking coefficient, sputtering yield, and incident current density must be such that the atom removal rate from the target exceeds the arrival and "sticking" rate from ambient. In general, low-mass ions have a lower sputtering yield for the targets investigated than do high-mass ions. It is for this reason that γ for the combination $Ne^+ \rightarrow$ Al was not measured. There was no assurance that the Al surface was clean even under the best vacuum conditions possible in the present system. The same would be true for lighter mass ions such as H^+, He^+, O^+, and N^+. Extending the present work must necessarily await major modification to reduce the ambient background pressure by at least one order of magnitude (to 10^{-9} Torr).

---

[11] L. N. Large, Proc. Phys. Soc. (London) **81**, 1101 (1963).

[12] N. N. Petrov and A. A. Dorozhkin, Ref. 1.

[13] V. G. Tel'kovskii, Izv. Akad. Nauk. SSSR **108**, 444 (1956) [English transl.: Soviet Phys.—Doklady **1**, 334 (1956)].

[14] N. R. Daly and R. E. Powell, Proc. Phys. Soc. (London) **84**, 595 (1964).